Blocking variability: Arctic Amplification versus Arctic Oscillation

Pedram Hassanzadeh[1] and Zhiming Kuang[2]

Corresponding author: P. Hassanzadeh, Center for the Environment, Harvard University, Cambridge, MA 02139, USA. (hassanzadeh@fas.harvard.edu)

[1]Center for the Environment and Department of Earth and Planetary Sciences, Harvard University, Cambridge, Massachusetts, USA.

[2]Department of Earth and Planetary Sciences and School of Engineering and Applied Sciences, Harvard University, Cambridge, Massachusetts, USA.

To predict future changes in blocking and the resulting weather extremes, some studies have proposed the negative phase of Arctic Oscillation (-AO) as an analogue for Arctic Amplification because of similarities between their mean-states: reduced midlatitude-to-pole temperature gradients and weakened, equatorward-shifted jet-streams. Using well-controlled modeling experiments, we show that blocking variations associated with mean-state anomalies are opposite depending on whether these anomalies are driven by the internal dynamics as in AO or forced externally as in Arctic Amplification. While blocking increases and its latitudinal-distribution shifts poleward in -AO, we find opposite responses when a mean-state identical to the -AO mean-state is externally forced. Findings suggest that the observed blocking-AO relationship is a correlation which does not imply that the -AO mean-state causes increased blocking, and should not be employed as a prototype for Arctic Amplification. Furthermore, results urge for a careful consideration of causality before using internal-variability to predict low-frequency response to external-forcings.

1. Introduction

Arctic Amplification has been one of the most prominent components of climate change in the past two decades and is a consistent feature of projected climates with increased green-house gases [*Cohen et al.*, 2014; *Vihma*, 2014; *Barnes and Polvani*, 2015; *Walsh*, 2014]. With Arctic Amplification, the near-surface midlatitude-to-pole temperature difference (ΔT_s) decreases, and the midlatitude jet weakens and shifts equatorward [*Cohen et al.*, 2014; *Barnes and Screen*, 2015; *Vihma*, 2014; *Francis and Vavrus*, 2012; *Liu et al.*, 2012; *Butler et al.*, 2010; *Hassanzadeh et al.*, 2014; *Barnes and Polvani*, 2015], although there are uncertainties in the latter [*Barnes and Screen*, 2015]. The potential influence of Arctic Amplification, and the associated changes in the cryosphere, on the midlatitude weather extremes has been a subject of intensive research in recent years [e.g., *Francis and Vavrus*, 2012; *Liu et al.*, 2012; *Barnes*, 2013; *Tang et al.*, 2013; *Mori et al.*, 2014; *Kim et al.*, 2014; *Screen et al.*, 2015; *Coumou et al.*, 2015; *Schneider et al.*, 2015]; however, the results have been largely inconclusive [see the reviews by *Cohen et al.*, 2014; *Vihma*, 2014; *Barnes and Screen*, 2015; *Walsh*, 2014; *Overland et al.*, 2015]. A major source of disagreement is uncertainties in how Arctic Amplification modulates the frequency and intensity of atmospheric blocks through changing ΔT_s and the speed and latitude of the midlatitude jet [see, e.g., *Cohen et al.*, 2014; *Vihma*, 2014; *Barnes and Screen*, 2015; *Overland et al.*, 2015; *Francis and Vavrus*, 2012; *Liu et al.*, 2012; *Barnes et al.*, 2014; *Woollings et al.*, 2014a; *Hassanzadeh et al.*, 2014; *Hoskins and Woollings*, 2015].

Blocking events, usually defined as large-scale persistent quasi-stationary high-pressure systems, can cause weather extremes such as heat waves, cold spells, droughts, and floods [e.g., *Dole et al.*, 2011; *Trigo et al.*, 2004; *Green*, 1977; *Lau and Kim*, 2012], which have dire consequences for the public health, economy, and ecosystem [*Barriopedro et al.*, 2011; *Robine et al.*, 2008; *Coumou and Rahmstorf*, 2012]. Despite numerous studies since the 1950s, how blocks form, persist beyond the synoptic timescale, and decay is still not well-understood [see *Tyrlis and Hoskins*, 2008, and references therein]. As a result of this incomplete theoretical understanding, short datasets [*Cohen et al.*, 2014], and the shortcomings of climate models [*Shepherd*, 2014; *Scaife et al.*, 2010; *Anstey et al.*, 2013; *Trenberth et al.*, 2015; *Ferranti et al.*, 2015], how blocks respond to changes in ΔT_s and the speed or latitude of the midlatitude jet, and hence the Arctic Amplification, remains unclear. To make progress in understanding and predicting changes in blocking despite these difficulties, some studies have proposed the negative phase of Arctic Oscillation (AO), an internal mode of climate variability, as an analogue for Arctic Amplification because of similarities between their atmospheric mean-states; see, e.g., Box 1 in *Cohen et al.* [2014].

AO (also known as the Northern Annular Mode) and its Southern Hemisphere counterpart, Antarctic Oscillation (AAO), are characterized by hemispheric north-south shifts of the extratropical circulation with an e-folding timescale of $\sim$ 10 days [*Thompson and Li*, 2015; *Thompson and Woodworth*, 2015], and exist due to the internal atmospheric dynamics, i.e., stochastic eddy-forcing and positive eddy-mean flow feedbacks [*Lorenz and Hartmann*, 2001; *Simpson et al.*, 2013; *Nie et al.*, 2014]. In Figure 1a we show the blocking statistics for $1950-2014$ Northern Hemisphere winters and summers in the NCEP-NCAR reanalysis divided based on whether the first day of a blocking event had a positive or negative AO index. In both seasons, blocking activity increases by factors of ~ 3 and shifts poleward in the negative phase of AO (denoted as -AO hereafter) compared to its positive phase (+AO), consistent with previous studies of AO [*Thompson and Wallace*, 2001; *Overland et al.*, 2015] and North Atlantic Oscillation (NAO) [*Woollings et al.*, 2014b; *Barriopedro et al.*, 2006] using other blocking indices. The same relationship exists between blocking activity and AAO, although the result is noisier due to shorter time-series (see Appendix B; also see *Oliveira et al.* [2013]).

These results might seem to suggest that the atmospheric mean-state associated with the -AO (and -AAO), i.e., equatorward-shifted midlatitude jets and weakened ΔT and midlatitude westerlies (see figures 2 in *Thompson and Li* [2015] and *Thompson and Woodworth* [2015]), is a condition that favors increased blocking activity [*Cohen et al.*, 2014; *Thompson and Wallace*, 2001]. Because of the similarities between the mean-state of the midlatitude atmosphere in the -AO and in response to Arctic Amplification, and in particular the resemblance between the -AO latitude-pressure pattern and the zonally-averaged zonal wind ($\bar{u}$) response to reduced sea-ice in many modeling studies [e.g., *Deser et al.*, 2015; *Peings and Magnusdottir*, 2011], -AO has been suggested as a prototype to understand how blocking activity might change with Arctic Amplification. The above line of reasoning would predict that Arctic Amplification increases blocking and shifts its latitudinal-distribution poleward.

The purpose of this study is to examine -AO as an analogue to understand and predict changes of blocking activity under Arctic Amplification, and to test whether there is a causal link between the -AO mean-state and increased blocking. We use well-controlled numerical experiments using an idealized general circulation model (GCM) and its linear response function. Results are shown in section 2 followed by discussions in section 3 and conclusions in section 4. The blocking index, reanalysis data, idealized model, and its linear response function are, respectively, described in Appendices A, B, C, and D at the end of the letter.

2. Results

Using -AO as an analogue for Arctic Amplification predicts increased and poleward-shifted blocking activity under Arctic Amplification; however, it has been recently shown that blocking activity decreases and shifts equatorward when the high-latitudes are forced to warm in an idealized atmospheric GCM, despite the decrease in ΔT_s and the speed and latitude of the midlatitude jet [*Hassanzadeh et al.*, 2014]. A summary of these results is shown in Figures 2a-2b in the same format that is used in this letter. The latitudinal-distributions of blocking frequency for two thresholds of the strength of blocking anomalies (1.5 and 2 standard deviation) for the control-run and for simulations with increased ΔT_s (i.e., forced high-latitudes cooling) and decreased ΔT_s (i.e., forced high-latitudes warming) are presented in these figures, which show a decrease in blocking activity as ΔT_s is reduced, i.e., under Arctic Amplification-like conditions. Furthermore, as ΔT_s changes, the latitudinal-distribution of blocking shifts in the same direction as the midlatitude jet, i.e., equatorward as ΔT_s decreases (see *Hassanzadeh et al.* [2014] for details).

These findings are consistent with observed changes of blocking frequency with the seasonal cycle: in the Northern Hemisphere winters versus summers, ΔT is larger, mid-latitude westerlies are faster (e.g., by a factor of $\sim$ 2 in maximum seasonal-mean $\bar{u}$, see Figure S1), while blocking is more frequent in winters, as shown in Figure 1b and reported previously with other blocking indices [*Barriopedro et al.*, 2006; *Wiedenmann et al.*, 2002]. Moreover, the midlatitude jets and blocking activity shift in the same direction, i.e., equatorward in winters compared to summers (Figures 1b and S1). The same changes in blocking activity are observed in the Southern Hemisphere winters and summers [*Wiedenmann et al.*, 2002].

Next, we compare the blocking-AO relationship in the control-run of the same simulations with the blocking-AO relationship in observations. As demonstrated in Figures 2c-2d, the blocking-AO relationship in the idealized model is the same as in observations (Figure 1a): blocking is more frequent, particularly at higher latitudes, in -AO compared to +AO. Therefore, reduced ΔT and jet's speed and latitude, when driven internally as in -AO, result in increased and poleward-shifted blocking activity, as schematically summarized in Figure 3a. However, in the same model, when the decrease in ΔT and jet's speed and latitude is forced externally, as under Arctic Amplification, blocking activity weakens and shifts equatorward (Figures 2a-2b), as summarized in Figure 3b. It should be clarified that Arctic Amplification can be affected by the internal-variability of the coupled climate-system on decadal (or shorter) timescales [e.g., *Wallace et al.*, 2012]; however, the focus here is on the long-term climate change-induced Arctic Amplification, which is externally forced.

These results suggest contrasting changes in blocking activity, both in magnitude and latitudinal-distribution, in response to the mean-states associated with -AO (internal-variability) and Arctic Amplification-like conditions (external-forcing), despite the similarities between the two mean-states. Such contrasting behaviors are not due to differences in the spatial patterns of the two mean-states, which, while similar, are not identical, either in the idealized simulations of Figure 2 or in the simulations with more complex GCMs (e.g., with reduced sea-ice) in other studies. This is illustrated by the following simulations whose mean-flow responses to specified external-forcings are almost identical to the -AO pattern. The -AO variability pattern in the idealized model, calculated using an Empirical Orthogonal Function (EOF) analysis of daily anomalous $\bar{u}$ and zonally-averaged temperature ($\bar{T}$), is shown in Figures 4a-4b. To force a zonally-averaged time-mean response in the mean-state that matches this variability pattern (i.e., to generate a permanent -AO pattern), we use the linear response function M of the idealized model to calculate a time-invariant zonally-symmetric forcing ($\bar{f}$) of $\bar{u}$ and $\bar{T}$ as $\bar{f} = -\mathsf{M}\bar{x}$, where $\bar{x}$ consists of the anomalous $\bar{u}$ and $\bar{T}$ shown in Figures 4a-4b (after normalization to have maximum $\bar{u} = 1$ m/s; see Appendix D for details). Five ensembles with different forcing amplitudes are run, which generate permanent -AO patterns that agree well with the variability patterns (see Figures 4c-4d). There are differences at small scales but the accuracy is adequate for the purpose of this experiment. Because the external-forcing $\bar{f}$ is time-invariant and zonally-symmetric, it affects zonally asymmetric phenomena such as blocking only indirectly through changing the mean-state, which is a suitable property for this experiment. Figures 4e-4f compare the blocking frequency of the control-runs with that of the forced-runs, showing that blocking activity decreases and shifts equatorward when reduced ΔT, equtorward-shifted jets, and weakened midlatitude westerlies are forced externally. These results are in agreement with the blocking-jet-ΔT relationship of Figure 3b, but opposite to the relationship when the same mean-state is generated by the internal atmospheric dynamics (Figure 3a).

3. Discussions

Results of Figures 2-4 show unequivocally that, on the contrary to a widely-used interpretation of observed blocking-AO/NAO relationship, a mean-state with reduced ΔT, equtorward-shifted midlatitude jets, and weakened midlatitude westerlies is not necessarily a condition that favors increased blocking activity. We emphasize that the blocking-AO/NAO relationship in observations and models is only a correlation and does not imply a causal relationship between blocking activity and the mean-state of AO (or NAO). For example, it is plausible that changes in synoptic eddies and wave-breaking events cause the changes both in mean-states and in blocking activities; see a recent re-examination of blocking-NAO relationship in *Woollings et al.* [2008].

Forcing by synoptic eddies has been shown to play a critical role in the persistence of blocking events by balancing the mean-flow advection [*Green*, 1977; *Shutts*, 1983; *Illari and Marshall*, 1983; *Trenberth*, 1986], and should be taken into account in any effort to understand changes in blocking activity. For example, ignoring eddy-forcing, one might expect mean-states with larger ΔT and faster westerlies to have less frequent blocking because it should be harder for the high-pressure anomalies to persist in one region (as required for blocks) when the mean-flow advection is stronger; however, such expectation is in contrast to the observed changes of blocking with the seasonal cycle (Figure 1b) and the results of modeling experiments (Figure 2a-2b and 4c-4d). Indeed larger ΔT not only results in faster westerlies, but also enhances baroclinicity and leads to stronger synoptic eddies and likely a greater forcing exerted on the anomalies against the mean-flow advection. Further understanding of the advection-eddy forcing balance requires a deep insight into the eddy-forcing mechanism, which is currently lacking. Additionally, understanding the contrasting blocking variations in -AO and under forced high-latitudes warming demands a complete assessment of differences between the synoptic-eddy activities in response to external-forcings on one hand [e.g., *Barnes and Thompson*, 2014; *Riviére*, 2011], and in the two phases of the annular modes (e.g., -AO) on the other [e.g., *Lorenz and Hartmann*, 2001; *Simpson et al.*, 2013; *Nie et al.*, 2014].

We emphasize that the goal of this study is to examine -AO as an analogue to predict changes of blocking activity under Arctic Amplification. For this purpose, the idealized model used here provides a dynamical framework to probe the Arctic Amplification-AO analogy and to test whether there is a causal link between the -AO mean-state and increased blocking. The model retains the physical processes that are known to be essential for the AO and blocking dynamics (i.e., synoptic eddies and eddy-mean flow interaction). Furthermore, the model reproduces the AO pattern fairly well, the blocking-AO relationship in the model is the same as in observation, and the response of blocking activity to forced high-latitudes warming is consistent with observed changes in blocking in response to another external-forcing, the seasonal cycle. The advantages of employing the idealized model are its simplicity and computational efficiency which allow us to isolate the effects of different phenomena (e.g., high-latitude warming), to obtain robust statistics, and to conduct well-controlled simulations particularly using the linear response function, hence circumventing some of difficulties associated with interpreting and understanding the observational data and outputs of full-physics GCMs. Of course as in any modeling study and as in any investigation of blocking statistics, the shortcomings and simplifications of the model (e.g, absence of moisture and realistic quasi-stationary planetary-wave patterns) and potential deficiencies of the blocking index should be kept in mind and the results have to be viewed with a degree of caution. In particular, the role of moist processes, which can modulate the AO and blocking dynamics (e.g., through latent heat release [*Pfahl et al.*, 2015]), should be addressed in future studies. A better understanding of eddy-blocking interaction, obtained through theoretical, hierarchical modeling, and observational efforts, will likely shed more light on the blocking-AO relationship.

We further emphasize that the results of this study do not directly address the question of how blocks change with Arctic Amplification, rather, they contribute to the ongoing research on this subject by providing evidence that a widely-used analogy, often employed due to the poor understanding of blocking dynamics, is invalid. A reliable conclusive prediction of blocking activity response to Arctic Amplification requires a hierarchy of modeling experiments to asses the role of the fundamental aspects of dry dynamics (as in *Hassanzadeh et al.* [2014]), quasi-stationary planetary-waves (e.g., using models with accurate representation of land-sea contrast and orography), ocean-atmosphere and troposphere-stratosphere couplings, and moist processes (which might affect blocking response by modulating changes in the mean-state [e.g., *Ceppi et al.*, 2014] and by warming the blocking air through latent heat release [*Pfahl et al.*, 2015]). It should be highlighted that all (or most) of these processes are present in full-physics GCMs; however, how blocks respond to Arctic Amplification in such models is unsettled [see *Barnes and Screen*, 2015;

Cohen et al., 2014; *Hoskins and Woollings*, 2015]. For instance, some studies [e.g., *Liu et al.*, 2012; *Kim et al.*, 2014; *Mori et al.*, 2014] have reported regional increases in blocking due to Arctic influence while several other studies [e.g., *Woollings et al.*, 2014a; *Barnes and Polvani*, 2015] have not found robust evidence for such a link. Furthermore, some studies have found that the mean-state response to reduced sea-ice is sensitive to the perturbation details and model setup [see, e.g., *Barnes and Screen*, 2015] as well as to the representation of the ocean [*Deser et al.*, 2015] and stratosphere [*Sun et al.*, 2015] in the model. Given that the mean-state influences the blocking response, such sensitivities and complexities hinder a reliable and conclusive prediction and understanding of how blocking changes with Arctic Amplification, and call for a hierarchical approach to this complicated problem [*Hassanzadeh et al.*, 2014; *Hoskins and Woollings*, 2015].

4. Conclusions

We present compelling evidence that the observed blocking-AO relationship is a correlation that does not imply that the -AO mean-state causes increased blocking, which suggests that -AO is not a suitable prototype to predict how blocking activity responds to Arctic Amplification. These results also suggest that employing AO to predict the response of other aspects of midlatitude circulation, such as the waviness of the jet-streams [*Cohen et al.*, 2014; *Francis and Vavrus*, 2015], to Arctic Amplification should be carefully examined. Furthermore, responses of the large-scale circulation to other external-forcings (e.g., due to climate change) also project onto AO or AAO [*Shepherd*, 2014; *Butler et al.*, 2010; *Ring and Plumb*, 2008] (for instance, stratospheric cooling due to ozone depletion projects onto +AAO [*Thompson and Solomon*, 2002; *Butler et al.*, 2010]). These similarities might encourage using the observed correlations of some atmospheric patterns with AO (or AAO) to predict future changes in phenomena such as extreme temperature or precipitation events; however, the analyses presented here demonstrate that such correlations might be misleading and lead to incorrect conclusions, particularly for poorly-understood phenomena such as blocking, if causality is not thoroughly considered.

Appendix A: Blocking Index

We use the two-dimensional height-based index that is described in details in *Hassanzadeh et al.* [2014]. Briefly, the index searches all grid points for positive daily-averaged 500 hPa height (Z500) anomalies that are larger than 1.5 (or 2 in Figure 2b) standard deviation for 7 days or longer, and produce easterlies on their equatorward-flank for at least one day. Calculations of anomalies and standard deviations are explained below for the observational and modeling data. To highlight the latitudinal shift of blocking distributions and changes in high-latitude blocks [*Overland et al.*, 2015; *Woollings et al.*, 2008], here statistics are reported as blocking frequency rather than blocking area (which was used in *Hassanzadeh et al.* [2014]); however, conclusions do not change if area is considered.

For Figure 1a and 2c-2d, percentage is calculated as the number of blocked days that start within a given range of AO index, averaged over all longitudes per latitudinal bins of 2.5^{o} (observation data) or 2.8^{o} (model data), and then divided by the total number of blocked days summed over all latitudes (of each hemisphere) $\times$100. For Figures 1b, 2a-2b, and 4e-4f, blocking frequency is calculated as the number of blocked days averaged over all longitudes per latitudinal bins (same as above) divided by the total number of analyzed days $\times 100$.

Appendix B: Reanalysis Data

For Figures 1 and S1, we use data from NCEP-NCAR reanalysis. Daily Z500 for $1950-2014$ on $2.5^{\circ} \times 2.5^{\circ}$ grid and seasonal-mean $\bar{u}$ for $1981-2014$ DJF and JJA are available at www.iridl.ldeo.columbia.edu. Daily Z500 anomalies at every grid point are calculated with respect to the seasonal-mean of each year's DJF or JJA. In each hemisphere, the maximum zonally-averaged Z500 standard deviation of all analyzed DJF months or all JJA months is used to normalize the anomalies. These numbers are $\sim$ 142 m (DJF) and $\sim$ 105 m (JJA) in the Northern Hemisphere and $\sim$ 121 m (DJF) and $\sim$ 135 m (JJA) in the Southern Hemisphere. Blocks are included in DJF or JJA statistics if their first day was in these months. Daily AO (AAO) index for $1950-2014$ $(1979-2014)$, calculated using an EOF analysis of 1000 hPa (700 hPa) height, is available at www.cpc.ncep.noaa.gov. In the Northern (Southern) hemisphere, the first days of blocking events are 3.4 (6.3) and 3 (2.3) times more frequently in -AO (-AAO) compared to +AO (+AAO) in DJF and JJA, respectively. Note that the blocking-AAO data are noisier because they are calculated from shorter time series, which is due to less frequent blocking and shorter observational records in the Southern Hemisphere compared to the Northern Hemisphere.

Appendix C: Idealized Model

We use the Geophysical Fluid Dynamics Laboratory dry dynamical core, which is a GCM for dry atmosphere, with Held-Suarez forcing [*Held and Suarez*, 1994]. The model is forced by Newtonian relaxation of temperature to a prescribed radiative equilibrium state with a specified equator-to-pole temperature difference ΔT_y. The setup is the same as in [*Hassanzadeh et al.*, 2014]. For Figures 2a-2d, spectral resolution T85 ($\sim 2.8^o \times 2.8^o$) with 30 equally-spaced vertical levels is used. For each ΔT_y, a three-member ensemble is generated, where the model is run for 40000 days for each member. $\Delta T_y = 40, 50, 60$ (control) , $70, 80$ K are used, but only results for $\Delta T_y = 40$ (red), 60 (black), and 80 K (blue) in Figures 2a-2b and for $\Delta T_y = 60$ K in Figures 2c-2d are shown for clarity and brevity. The results of Figures 2a-2d are from simulations with zonally-symmetric lower boundary conditions. Similar distributions and the same blocking-jet-ΔT relationships as Figures 3a-3b are obtained for the same configurations but with a 4 km mountain added to 45^o latitude in each hemisphere. Mountains are approximately Gaussian with widths 45^o (longitude) $\times 15^o$ (latitude).

AO is the leading mode of variability in this model and its spatial pattern (Figures 4a-4b) agrees reasonably well with observations (figures 2 in *Thompson and Li* [2015] and *Thompson and Woodworth* [2015]), particularly in the Southern Hemisphere [*Thompson and Woodworth*, 2015] where the lower boundary-condition is more zonally symmetric. In the model, the first EOF of zonally-averaged daily surface pressure explains $\sim 70\%$ of the variance, and its principal component time-series, normalized by its standard deviation, is used to calculate the daily AO index for Figures 2c-2d.

For Figure 4, ΔT_y is 60 K, resolution is T63 ($\sim 1.9^o \times 1.9^o$) with 40 equally-spaced vertical levels, and each member of the ensemble is run for 45000 days. For Figures 4a-4b, the -AO pattern is calculated as the first EOF of daily $\bar{u}$ and $\bar{T}$ (combined for the analysis), which explains $\sim$ 49% of the variance (regressing daily $\bar{u}$ and $\bar{T}$ on the AO index calculated above from surface pressure yields a similar pattern). For Figures 4c-4f, zonally-symmetric time-invariant forcings $\bar{f}$ in $\bar{u}$ and $\bar{T}$ are applied to force the mean-flow response to match the first EOF of $(\bar{u}, \bar{T})$ with specified amplitudes (see Appendix D for details).

For the blocking statistics in Figures 2 and 4, 6 h outputs are first interpolated to a T42 grid ($\sim 2.8^{\mathrm{o}} \times 2.8^{\mathrm{o}}$). Daily-averaged Z500 anomalies are calculated with respect to time-mean Z500 and normalized using the maximum zonal-mean Z500 standard deviation of each run. The standard deviation decreases with ΔT_y [*Hassanzadeh et al.*, 2014], e.g., it is $\sim$ 1.7 times larger for the runs with $\Delta T_y = 80$ K compared to the runs with $\Delta T_y =$ 40 K. The decrease of standard deviation with reduced meridional temperature gradient is consistent with observation [*Screen*, 2014] and theory [*Schneider et al.*, 2015]. As discussed in [*Hassanzadeh et al.*, 2014], the trends reported in Figures 2a-2b are not sensitive to using the standard deviation of each run to normalize the anomalies. In fact blocking increases with ΔT_y despite the fact that the anomalies are normalized by increasingly larger standard deviations. This is also true for the seasonal cycle in reanalysis data: more blocks are found in winters compared to summers (Figure 1b) despite normalization with larger standard deviations (see Appendix B).

Appendix D: Linear Response Function

The linear response function M relates the zonally-averaged response state-vector $\bar{x}$ to its tendency $\dot{\bar{x}}$ and a zonally-symmetric external-forcing $\bar{f}$ as [*Palmer*, 1999; *Kuang*, 2010;

Ring and Plumb, 2008]

$$\dot{\bar{x}} = \mathsf{M}\bar{x} + \bar{f}. \tag{D1}$$

In the current study, $\bar{x}$ includes $\bar{u}$ and $\bar{T}$ responses, i.e., deviations from the climatology of the unforced (control) runs. M represents advection, frictional and diabatic processes, and turbulent eddy-feedback. The eddy-feedback, for which no complete theory exists, is vital for an accurate calculation of M [*Ring and Plumb*, 2008]. To compute M for the dry dynamical core with the eddy-feedback included, we employ the framework described in *Kuang* [2010] for a cloud-resolving model. Briefly, time-independent zonally-symmetric forcings in $\bar{u}$ or $\bar{T}$ are imposed, one at a time, at 100 latitude-pressure locations: every 10^{o} from 0^{o} to 90^{o}, and every 100 hPa from 1000 hPa to 100 hP. The spatial profile of each forcing, applied simultaneously in both hemispheres, is Gaussian with standard deviations of $\sim 7.1^{\text{o}}$ and ~ 53 hPa. The amplitude of each forcing is chosen to be large enough to obtain an acceptable signal-to-noise ratio, yet small enough for the response to be a linear function of forcing.

For each forced-run, after 500 days of spin-up, a 44500-day integration is used to calculate the zonally-averaged time-mean response in $\bar{u}$ and $\bar{T}$ with respect to the control-run (a 45000-day unforced-run). Each response is averaged between the two hemispheres. To improve accuracy, for each forcing, positive and negative amplitudes are used (leading to 400 total forced-runs) and the responses are combined (200 total forcing-response sets) and then projected onto the 100 Gaussian profiles (described above) using least-square linear regression. The 200 regression coefficients of each response (for $\bar{u}$ and $\bar{T}$ combined) form one column of matrix X and the corresponding forcing amplitude forms the same column of matrix F (see *Kuang* [2010]). The left-hand side of equation (1) vanishes due to long-time averaging and $\mathsf{M} = -\mathsf{F}\mathsf{X}^{-1}$ is calculated using direct matrix inversion. M has been calculated for $\Delta T_y = 60$ K and resolution T63 with 40 vertical levels.

To calculate the forcings $\bar{f}$ used in Figures 4c-4f, the first EOF of $(\bar{u}, \bar{T})$, shown in Figures 4a-4b, is normalized to have maximum $\bar{u} = 1$ m/s, and then projected onto the same 100 Gaussian profiles described above. The 200 regression coefficients form vector $\bar{x}$, and $\bar{f} = -\mathsf{M}\bar{x}$ is calculated. Five ensembles forced with $a \times \bar{f}$ (with $a = 2, 3, 4, 5$ and 6) are run, but only results for $a = 3$ and 6 are shown for clarity.

Acknowledgments. We thank Elizabeth Barnes, Judah Cohen, and Jennifer Francis for fruitful discussions; Elizabeth Barnes, Karen McKinnon, Andy Rhines, and Marty Singh for insightful comments on the manuscript; and Ding Ma and Chris Walker for useful suggestions on data analysis and modeling experiments. This work was supported by a Ziff Environmental Fellowship from the Harvard University Center for the Environment to P.H and NSF grant AGS-1062016 to Z.K. The simulations were run on Harvard Odyssey cluster. The data for this paper are available upon request.

References

Anstey, J. A., P. Davini, L. J. Gray, T. J. Woollings, N. Butchart, C. Cagnazzo, and S. Yang (2013), Multi-model analysis of Northern Hemisphere winter blocking: Model biases and the role of resolution, *J. Geophys. Res.*, *118*(10), 3956–3971.

Barnes, E. A. (2013), Revisiting the evidence linking Arctic amplification to extreme weather in midlatitudes, *Geophys. Res. Lett.*, *40*(17).

Barnes, E. A., E. Dunn-Sigouin, G. Masato, and T. Woollings (2014), Exploring recent trends in Northern Hemisphere blocking, *Geophys. Res. Lett.*, *41*.

Barnes, E. A. and D. W. J. Thompson (2014), Comparing the roles of barotropic versus baroclinic feedbacks in the atmospheres response to mechanical forcing, *J. Atmos. Sci.*, *71*(1), 177–194 doi:10.1175/JAS-D-13-070.1.

Barnes, E. A., and J. A. Screen (2015), The impact of Arctic warming on the midlatitude jet-stream: Can it? Has it? Will it? *WIREs Clim. Change*, *6*, 277-286 doi:10.1002/wcc.337.

Barnes, E. A., and L. M. Polvani (2015), CMIP5 projections of Arctic amplification, of the North American/North Atlantic circulation, and of their relationship, *J. Climate*, *28*, 5254-5271 doi:10.1175/JCLI-D-14-00589.1.

Barriopedro, D., R. García-Herrera, A. R. Lupo, and E. Hernndez (2006), A climatology of Northern Hemisphere blocking, *J. Climate*, *19*(6), doi:10.1175/JCLI3678.1.

Barriopedro, D., E. M. Fischer, J. Luterbacher, R. M. Trigo, and R. Garca-Herrera (2011), The hot summer of 2010: redrawing the temperature record map of Europe, *Science*, *332*(6026), 220–224 doi:10.1126/science.1201224.

Butler, A. H., D. W. Thompson, and R. Heikes (2010), The steady-state atmospheric circulation response to climate change-like thermal forcings in a simple general circulation model, *J. Climate*, *23*(13), 3474-3496 doi:10.1175/2010JCLI3228.1.

Ceppi, P., M. D. Zelinka, and D. L. Hartmann (2014), The response of the Southern Hemispheric eddy-driven jet to future changes in shortwave radiation in CMIP5, *Geophys. Res. Lett.*, *41*.

Cohen, J. *et al.* (2014), Recent Arctic amplification and extreme mid-latitude weather, *Nat. Geosci.*, *7*, 627–637 doi:10.1038/ngeo2234.

Coumou, D., and S. Rahmstorf (2012), A decade of weather extremes, *Nat. Clim. Change*, *2*, 491–496 doi:10.1038/nclimate1452.

Coumou, D., J. Lehmann and J. Beckmann (2015), The weakening summer circulation in the Northern Hemisphere mid-latitudes, *Science*, *348*, 324–327 doi: 10.1126/science.1261768.

Deser, C., R. A. Tomas, and L. Sun (2015), The role of ocean-atmosphere coupling in the zonal mean atmospheric response to Arctic sea ice loss, *J. Climate*, *28*, 2168-2186 doi:10.1175/JCLI-D-14-00325.1.

Dole, R., M. Hoerling, J. Perlwitz, J. Eischeid, P. Pegion, T. Zhang, and D. Murray (2011), Was there a basis for anticipating the 2010 Russian heat wave?, *Geophys. Res. Lett.*, *38*(6).

Ferranti, L., S. Corti, and M. Janousek (2015), Flow-dependent verification of the ECMWF ensemble over the Euro-Atlantic sector, *Q. J. R. Meteorol. Soc.*, *141*, 916-924 doi:10.1002/qj.2411.

Francis, J. A., and S. J. Vavrus (2012), Evidence linking Arctic amplification to extreme weather in mid-latitudes, *Geophys. Res. Lett.*, *39*(6).

Francis, J. A. and S. J. Vavrus (2015), Evidence for a wavier jet stream in response to rapid Arctic warming, *Environ. Res. Lett.*, *10*, doi:10.1088/1748-9326/10/1/014005.

Green, J. S. A. (1977), The weather during July 1976: Some dynamical considerations of the drought, *Weather*, *32*(4), 120–126.

Hassanzadeh, P., Z. Kuang, and B. F. Farrell (2014), Responses of midlatitude blocks and wave amplitude to changes in the meridional temperature gradient in an idealized dry GCM, *Geophys. Res. Lett.*, *41*.

Held, I. M. and M. J. Suarez (1994), A proposal for the intercomparison of the dynamical cores of atmospheric general circulation models, *Bull. Am. Meteorol. Soc.*, *75*(10), 1825–1830.

Hoskins, B. and T. Woollings (2015), Persistent extratropical regimes and climate extremes, *Current Climate Change Reports*, *1*, 115–124 doi:10.1007/s40641-015-0020-8.

Illari, L. and J. C. Marshall (1983), On the interpretation of eddy fluxes during a blocking episode, *J. Atmos. Sci.*, *40*, 2232–2242.

Kim, B. M., S. W. Son, S. K. Min, J. H. Jeong, S. J. Kim, X. Zhang, T. Shim, and J. H. Yoon (2014), Weakening of the stratospheric polar vortex by Arctic sea-ice loss, *Nat. Commun.*, *5*, doi:10.1038/ncomms5646.

Kuang, Z. (2010), Linear response functions of a cumulus ensemble to temperature and moisture perturbations and implications for the dynamics of convectively coupled waves, *J. Atmos. Sci.*, *67*, 941-962 doi:10.1175/2009JAS3260.1.

Lau, W. K. and K. M. Kim (2012), The 2010 Pakistan flood and Russian heat wave: Teleconnection of hydrometeorological extremes, *J. Hydrometeorol.*, *13*, 392–403 doi:10.1175/JHM-D-11-016.1.

Liu, J., J. A. Curry, H. Wang, M. Song, and R. M. Horton (2012), Impact of declining Arctic sea ice on winter snowfall, *Proc. Natl. Acad. Sci.*, *109*(11), 4074–4079 doi:10.1073/pnas.1114910109.

Lorenz, D. J. and D. L. Hartmann (2001), Eddy-zonal flow feedback in the Southern Hemisphere, *J. Atmos. Sci.*, *58*, 3312–3327 doi:10.1175/1520-0469(2001)058¡3312:EZFFIT¿2.0.CO;2.

Mori, M., M. Watanabe, H. Shiogama, J. Inoue, and M. Kimoto (2014), Robust Arctic sea-ice influence on the frequent Eurasian cold winters in past decades, *Nat. Geosci.*, *7*, 869-873 doi:10.1038/ngeo2277.

Nakamura, H., M. Nakamura, and J. L. Anderson (1997), The role of high- and low-frequency dynamics in blocking formation, *Mon. Weather Rev.*, *125*(9), 2074–2093.

Nie, Y., Y. Zhang, G. Chen, X. Q. Yang, and D. A. Burrows (2014), Quantifying barotropic and baroclinic eddy feedbacks in the persistence of the Southern Annular Mode, *Geophys. Res. Lett.*, *41*(23).

Oliveira, F. N. M, L. M. V. Carvalho, and T. Ambrizzi (2013), A new climatology for Southern Hemisphere blockings in the winter and the combined effect of ENSO and SAM phases. *Int. J. Climatol.*, *34*(5), 1676–1692.

Overland, J., J. A. Francis, R. Hall, E. Hanna, S.-J. Kim, and T. Vihma (2015), The Melting Arctic and Mid-latitude Weather Patterns: Are They Connected? *J. Climate*, doi:10.1175/JCLI-D-14-00822.1.

Palmer, T. N (1999), A nonlinear dynamical perspective on climate prediction, *J. Climate*, *12*, 575–591 doi:10.1175/1520-0442(1999)012¡0575:ANDPOC¿2.0.CO;2.

Peings, Y., and G. Magnusdottir (2014), Response of the wintertime Northern Hemisphere atmospheric circulation to current and projected Arctic sea ice decline: A numerical study with CAM5, *J. Climate*, *27*(1), 244-264 doi:10.1175/JCLI-D-13-00272.1.

Pelly, J. L. and B. J. Hoskins (2003), A new perspective on blocking, *J. Atmos. Sci.*, *60*(5), 743-755 doi:10.1175/1520-0469(2003)060¡0743:ANPOB¿2.0.CO;2.

Pfahl, S., C. Schwierz, M. Croci-Maspoli, C. M. Grams, and H. Wernli (2015), Importance of latent heat release in ascending air streams for atmospheric blocking, *Nat. Geosci.*, *8*(8), 610–614 doi:10.1038/ngeo2487.

Ring, M. J. and R. A. Plumb (2008), The response of a simplified GCM to axisymmetric forcings: Applicability of the fluctuation-dissipation theorem, *J. Atmos. Sci.*, *65*, 3880–3898 doi:10.1175/2008JAS2773.1.

Riviére, G. (2011), A Dynamical interpretation of the poleward shift of the jet streams in global warming scenarios, *J. Atmos. Sci.*, *68*(6) doi:10.1175/2011JAS3641.1.

Robine, J. M., S. L. K. Cheung, S. Le Roy, H. Van Oyen, C. Griffiths, J. P. Michel, and F. R. Herrmann (2008), Death toll exceeded 70,000 in Europe during the summer of 2003, *C. R. Biol.*, *331*(2), 171–178 doi:10.1016/j.crvi.2007.12.001.

Scaife, A. A., D. Copsey, C. Gordon, C. Harris, T. Hinton, S. Keeley, A. OŃeill, M. Roberts, and K. Williams (2010), Improved Atlantic winter blocking in a climate model, *Geophys. Res. Lett.*, *38*.

Schneider, T., T. Bischoff, and H. Plotka (2015), Physics of changes in synoptic midlatitude temperature variability, *J. Climate*, *28*, 2312-2331 doi:10.1175/JCLI-D-14-00632.1.

Screen, J. A. (2014), Arctic amplification decreases temperature variance in northern mid- to high-latitudes, *Nat. Clim. Change*, *4*, 577-582 doi:10.1038/NCLIMATE2268.

Screen, J. A., C. Deser, and L. Sun (2014), Reduced risk of North American cold extremes due to continued sea ice loss, *Bull. Amer. Met. Soc.*, doi:10.1175/BAMS-D-14-00185.1.

Shepherd, T. G. (2014), Atmospheric circulation as a source of uncertainty in climate change projections, *Nat. Geosci.*, *7*, 703-708 doi:0.1038/ngeo2253.

Shutts, G. J. (1983), The propagation of eddies in diffluent jetstreams: Eddy vorticity forcing of blocking flow fields, *Q. J. R. Meteorol. Soc.*, *109*, 737–761.

Simpson, I. R., T. G. Shepherd, P. Hitchcock, and J. F. Scinocca (2013), Southern annular mode dynamics in observations and models. Part II: Eddy feedbacks, *J. Climate*, *26*(14), 5220–5241 doi:10.1175/JCLI-D-12-00495.1.

Sun, L., C. Deser, and R. A. Tomas (2015), Mechanisms of stratospheric and tropospheric circulation response to projected Arctic sea ice loss, *J. Climate*, doi:10.1175/JCLI-D-15-0169.1.

Tang, Q., X. Zhang, and J. A. Francis (2013a), Extreme summer weather in northern mid-latitudes linked to a vanishing cryosphere, *Nat. Clim. Change*, *4*, 45–50 doi:10.1038/nclimate2065.

Thompson, D. W. J. and J. M. Wallace (2001), Regional climate impacts of the Northern Hemisphere annular mode, *Science*, *293*, 85–89 doi:10.1126/science.1058958.

Thompson, D. W. J. and S. Solomon (2002), Interpretation of recent Southern Hemisphere climate change, *Science*, *296*, 895–899 doi:10.1126/science.1069270.

Thompson, D. W. J. and L. Li (2015), Barotropic and baroclinic annular variability in the Northern Hemisphere, *J. Atmos. Sci.*, *72*, 1117–1136 doi:10.1175/JAS-D-14-0104.1.

Thompson, D. W. J. and J. D. Woodworth (2015), Barotropic and baroclinic annular variability in the Southern Hemisphere, *J. Atmos. Sci.*, *71*, 1480-1493 doi:10.1175/JAS-D-13-0185.1.

Trenberth, K. E. (1986), An assessment of the impact of transient eddies on the zonal flow during a blocking episode using localized Eliassen-Palm flux diagnostics, *J. Atmos. Sci.*, *43*(19), 2070–2087.

Trenberth, K. E., J. T. Fasullo, and T. G. Shepherd (2015), Attribution of climate extreme events, *Nat. Clim. Change*, doi:10.1038/nclimate2657.

Trigo, R. M., I. F. Trigo, C. C. DaCamara, and T. J. Osborn (2004), Climate impact of the European winter blocking episodes from the NCEP/NCAR Reanalyses, *Clim. Dynam.*, *23*(1), 17–28 doi:10.1007/s00382-004-0410-4.

Tyrlis, E., and B. J. Hoskins (2008), Aspects of a Northern Hemisphere atmospheric blocking climatology, *J. Atmos. Sci.*, *65*(5) doi:10.1175/2007JAS2337.1.

Vihma, T. (2014), Effects of Arctic sea ice decline on weather and climate: A review, *Surv. Geophys.*, 1–40 doi:10.1007/s10712-014-9284-0.

Wallace, J. M., Q. Fu, B. V. Smoliak, P. Lin, and C. M. Johanson (2012), Simulated versus observed patterns of warming over the extratropical Northern Hemisphere continents during the cold season, *Proc. Natl. Acad. Sci.*, *109*(36), 14337–14342 doi:10.1073/pnas.1204875109.

Walsh, J. E. (2014), Intensified warming of the Arctic: Causes and impacts on middle latitudes, *Glob. Planet. Change*, *117*, 52-63 doi:10.1016/j.gloplacha.2014.03.003.

Wiedenmann, J. M., A. R. Lupo, I. I. Mokhov, and E. A. Tikhonova (2002), The climatology of blocking anticyclones for the Northern and Southern Hemispheres: Block intensity as a diagnostic, *J. Climate*, *15*, 3459–3473 doi:10.1175/1520-0442(2002)015¡3459:TCOBAF¿2.0.CO;2.

Woollings, T., B. J. Hoskins, M. Blackburn, M., and P. Berrisford (2008), A new Rossby wavebreaking interpretation of the North Atlantic Oscillation, *J. Atmos. Sci.*, *65*(2), 609-626 doi:10.1175/2007JAS2347.1.

Woollings, T., B. Harvey, and G. Masato (2014a), Arctic warming, atmospheric blocking and cold European winters in CMIP5 models, *Environ. Res. Lett.*, *9*(1), doi: 10.1088/1748-9326/9/1/014002.

Woollings, T., C. Franzke, D. L. R. Hodson, B. Dong, E. A. Barnes, C. C. Raible, and J. G. Pinto (2014b), Contrasting interannual and multidecadal NAO variability, *Clim. Dyn.*, *45*, 1–18 doi:10.1007/s00382-014-2237-y.

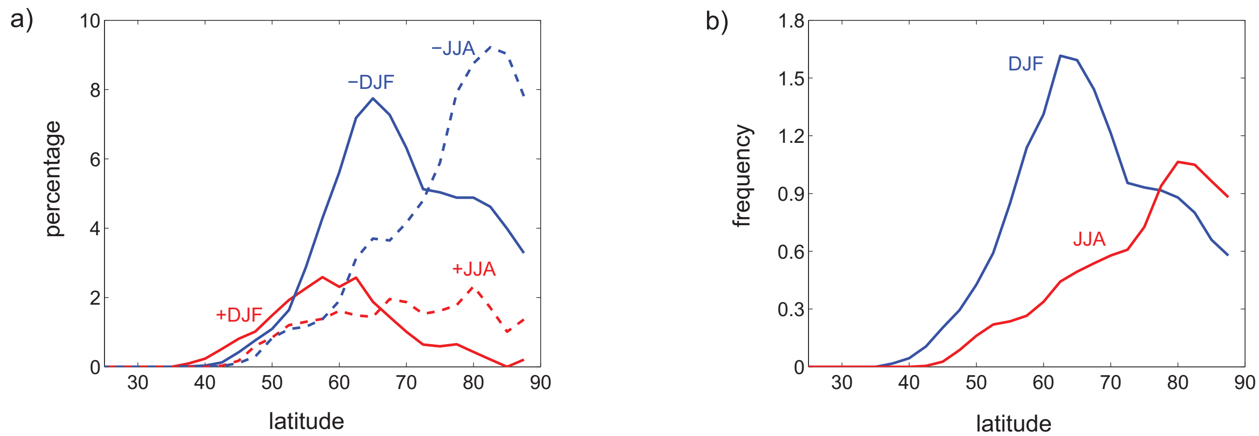

Figure 1. Blocking in the Northern Hemisphere for $1950 - 2014$ winters (December-January-February, DJF) and summers (June-July-August, JJA) in the NCEP-NCAR reanalysis. a) percentage (%) of blocks that start on days when the AO index is positive (+DJF and +JJA) or negative (-DJF and -JJA). Summed over all latitudes, ratios of blocks in -AO relative to +AO are ~ 3.4 (DJF) and ~ 3 (JJA). Similar distributions and the same conclusions are reached if the statistics are calculated using the AO index of every blocked day rather than only the index of the first day of blocking events, and/or if only blocks that start on days with AO index ≤ -1 and $\geq +1$ were considered. b) seasonal distribution of blocking frequency (%). All latitudes considered, blocking is ~ 1.7 times more frequent in winter compared to summer. See Appendices A and B for details.

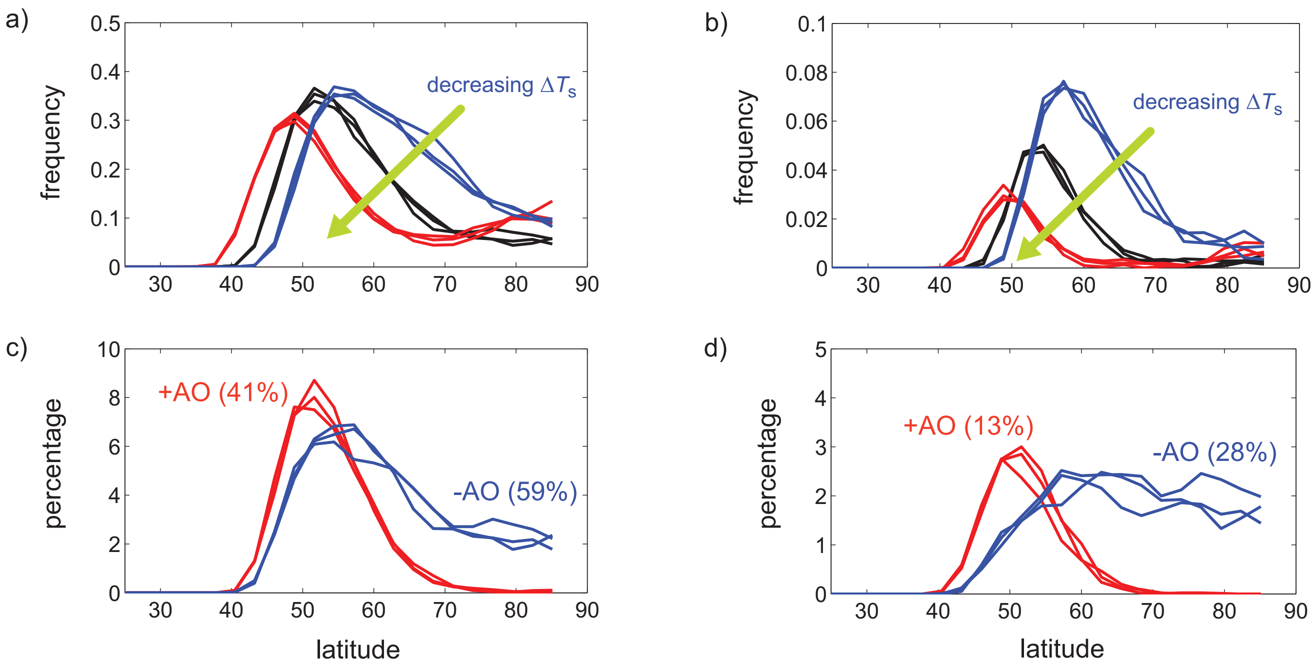

Figure 2. Blocking in idealized modeling experiments. a) blocking frequency (%) for 500 hPa height (Z500) anomalies ≥ 1.5 standard deviation in three-member ensemble runs with decreased ΔT_s (red) and increased ΔT_s (blue) compared to the control-runs (black). b) same as (a) but for stronger blocks (≥ 2 standard deviation). Percentage (%) of blocks in the control-runs that start on days when the AO index is positive (red) or negative (blue) (c), and when the index is ≤ -1 (red) or $\geq +1$ (blue) (d). Parentheses show the ensemble-mean percentages summed over all latitudes. Similar distributions and the same conclusions are reached if the statistics are calculated using the AO index of every blocked day, and also for cases with increased or decreased ΔT_s. See Appendices A and C for details.

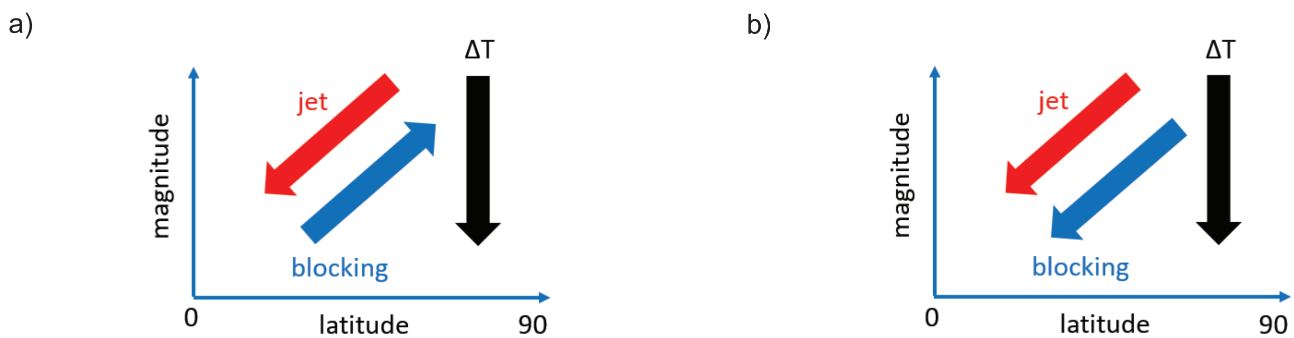

Figure 3. Schematic relationship between the midlatitude-to-pole temperature difference (ΔT), magnitude (speed) and latitude of the midlatitude jet, and the magnitude and latitudinal-distribution of blocking activity in -AO (a), and under Arctic Amplification-like conditions (b). Note that only the first-order changes in ΔT and jet's speed/latitude are shown to facilitate side-by-side comparisons; the spatial patterns of these changes are indeed more complex, see Figures 4a-4d and *Hassanzadeh et al.* [2014] (Figure S3).

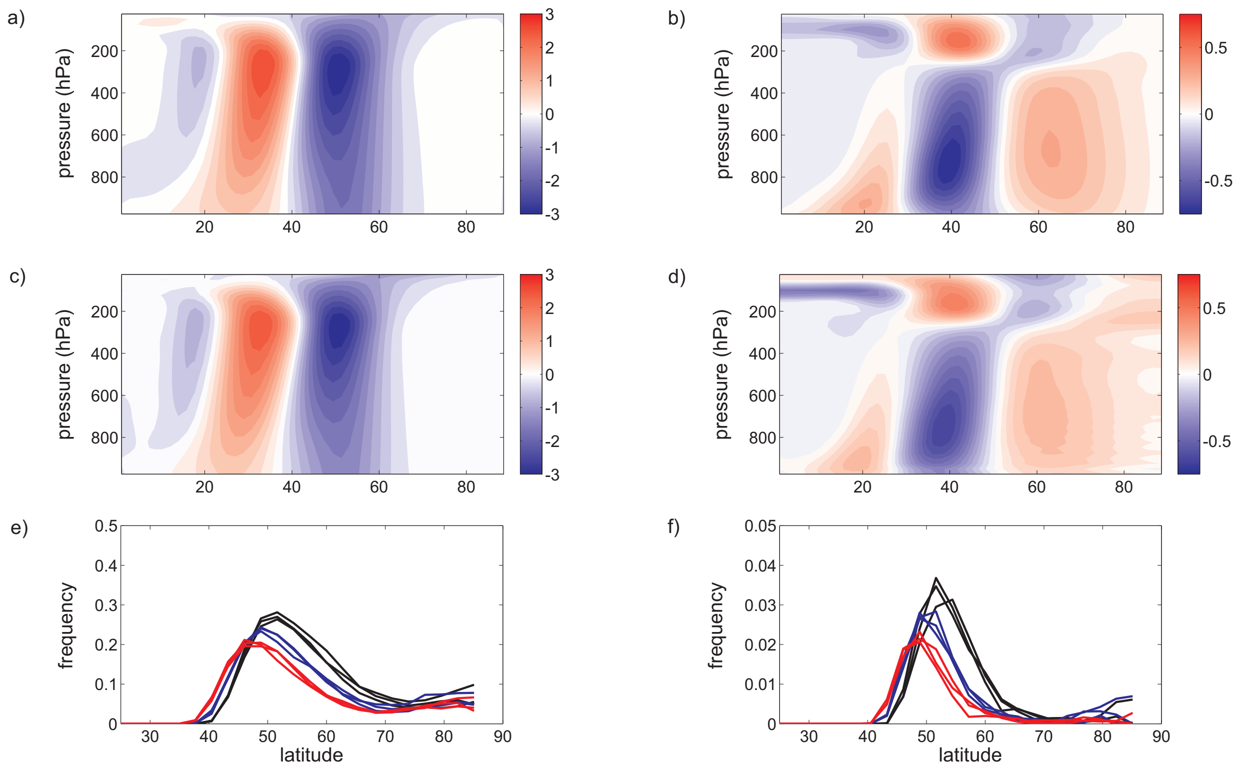

Figure 4. The -AO variability and permanent patterns in the idealized experiments. The first EOF of $\bar{u}$ (a) and $\bar{T}$ (b) in the control-run is the -AO variability pattern (scaled to have maximum $\bar{u} = 3$ m/s). Time-mean response of $\bar{u}$ (c) and $\bar{T}$ (d) in the run forced with $3\bar{f}$ is the permanent -AO pattern. As discussed in the text and in Appendix D, $\bar{f}$ is calculated using the linear response function so that the permanent pattern matches the variability pattern. Blocking frequency (%) in the control-runs (black) and runs forced with $3\bar{f}$ (blue) and $6\bar{f}$ (red) for Z500 anomalies that are ≥ 1.5 standard deviation (e) and ≥ 2 standard deviation (f). The ensemble-mean frequency, summed over all latitudes, decreases by factors of ~ 0.7 (e) and 0.6 (f) for the runs with $6\bar{f}$ compared to the control-runs. See Appendices A, C, and D for details.